JCTC Journal of Chemical Theory and Computation

Article

pubs.acs.org/JCTC

# QTAIM Analysis in the Context of Quasirelativistic Quantum Calculations

Julien Pilmé,*[,†,‡] Eric Renault,[§] Fadel Bassal,[§] Mohamed Amaouch,[†,‡] Gilles Montavon,[#] and Nicolas Galland*[,§]

[†]Laboratoire de Chimie Théorique, Sorbonne Universités, UPMC Université Paris 06, UMR 7616, F-75005 Paris, France

[‡]Laboratoire de Chimie Théorique, CNRS UMR 7616, F-75005 Paris, France

[§]CEISAM, UMR CNRS 6230, Université de Nantes, 2 Rue de la Houssinière, BP 92208, 44322 Nantes Cedex 3, France

[#]SUBATECH, UMR CNRS 6457, IN2P3/EMN Nantes/Université de Nantes, 4 rue A. Kastler, BP 20722, 44307 Nantes Cedex 3, France

Supporting Information

**ABSTRACT:** Computational chemistry currently lacks ad hoc tools for probing the nature of chemical bonds in heavy and superheavy-atom systems where the consideration of spin−orbit coupling (SOC) effects is mandatory. We report an implementation of the Quantum Theory of Atoms-In-Molecules in the framework of two-component relativistic calculations. Used in conjunction with the topological analysis of the Electron Localization Function, we show for astatine (At) species that SOC significantly lowers At electronegativity and boosts its propensity to make charge-shift bonds. Relativistic spin-dependent effects are furthermore able to change some bonds from mainly covalent to charge-shift type. The implication of the disclosed features regarding the rationalization of the labeling protocols used in nuclear medicine for $^{211}$At radioisotope nicely illustrates the potential of the introduced methodology for investigating the chemistry of (super)heavy elements.

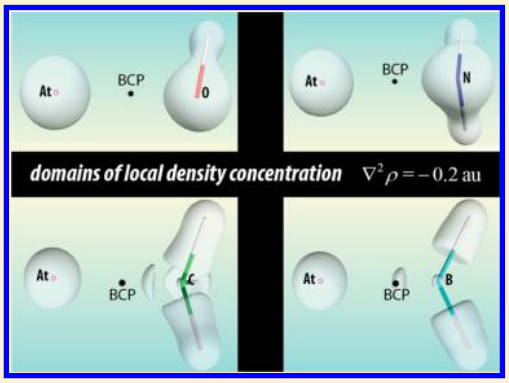


## 1. INTRODUCTION

It is generally acknowledged that relativistic quantum treatments must be used for studying the chemistry of compounds that contain heavy atoms. While relativistic methods have undergone significant developments and considerable progress have been achieved during the last 20 years in applying such methods to molecular systems of increasing size,[1−7] chemists currently lack ad hoc tools for probing the bonding nature in these systems. Indeed, the molecular structure and bonding can be strongly modified by relativistic effects. Relativistic effects are defined as the resulting differences between relativistic and nonrelativistic calculations. One may distinguish between electron spin-independent (scalar) and spin-dependent relativistic effects. The main spin-dependent effect is the spin−orbit coupling (SOC), which may become as important as scalar effects for heavy *p*-elements. The scalar effects are associated with the relativistic mass increase of electrons, resulting essentially from their high speed in the vicinity of heavy nuclei. The latter can be incorporated into existing nonrelativistic programs with minimum extra code developments. Therefore, most of the tools developed for years by theoreticians are available for investigating scalar-relativistic effects on our traditional pictures of the chemical bond. The most important outcomes can readily be traced in the literature covering the past decades.[8,9] The situation is deeply contrasting with respect to the studies of SOC effects on chemical bonding.

While some major trends have been uncovered,[10−25] the influence of SOC on bonding schemes has been hardly studied. Even if there is a growing interest in studying compounds involving heavy and superheavy atoms using relativistic calculations of increasing sophistication (to account for all relativistic effects), striking examples can readily be found in the literature[26−29] showing that the currently most adopted approach to investigate the chemical bonding in such compounds is to switch to a scalar-relativistic level. A fundamental problem is that chemists are not familiar with spinors, which are usually used to expand SOC wave functions. A spinor is nothing but a specific type of orbital, but the spinors do not lend themselves easily to visualization (as they are complex vector functions). Seminal works intended to reveal the fundaments of the modifications, due to SOC effects, on the bonding schemes were discussed in term of spinors. It was rationalized for homonuclear diatomic molecules that SOC mixes molecular orbitals (MOs) of different symmetries ($\sigma$ and $\pi$) and therefore reduces the bond strength.[10,13,30] Changes have been noticed in the weights of covalent and ionic forms

**Received:** July 17, 2014
**Published:** September 25, 2014

   dx.doi.org/10.1021/ct500762n | *J. Chem. Theory Comput.* 2014, 10, 4830−4841

used to describe the bond of heteronuclear diatomic molecules, due to the splitting of atomic p shells in $p_{1/2}$ and $p_{3/2}$ atomic spinors.[12,31] Regarding heavy atom molecules, examples are also reported for which the valence shell electron pair repulsion (VSEPR) structure is also influenced by Jahn−Teller distortions.[14−16,23−25] Note that these works are limited to small systems as they heavily rely on the use of molecular or local symmetry. The use of canonical molecular spinors, like done in MO theory, appears to hinder the bonding analysis, especially for complex systems as opposed to small and/or symmetric model systems. Other ways to proceed exist, for instance Saue et al. have notably promoted the use of localized spinors in the context of relativistic quantum computations.[18] Suitable localization criteria are able to recover some chemical significance in terms of bonding, lone pairs, and core orbitals. Following this route, natural spinors (similar to natural orbitals in nonrelativistic frameworks) have been derived and implemented.[32,33] Some may argue that the analysis of bonding schemes should not, as far as possible, rely on molecular spinors/orbitals since they are not observables and since the choice of their representation (canonical, natural, or other localized forms) may lead to different pictures. Alternative strategies exist in the field of nonrelativistic quantum calculations. They use topological analyzes to scrutinize the breaking and formation of bonds between atoms, for instance of the Electron Localization Function (ELF), first defined by Becke and Edgecombe[34] and which is a signature of the distribution of electronic pairs. Because the analysis of its topology is powerful to characterize bonding schemes,[35] this approach has been intensively used in recent years.[36,37] Some of us have notably introduced the ELF topological analysis in the field of two-component (2c) relativistic treatments.[38] The new formalism allows chemists to study large molecular systems for which the consideration of SOC is crucial. Following this route, we present in this article an implementation of the Quantum Theory of Atoms-In-Molecules (QTAIM) in the context of 2c quantum calculations (or quasirelativistic quantum calculations). Introduced back in 1970s by Richard F. W. Bader, QTAIM provides the theoretical framework for studying the topology of the total electron density, $\rho(\mathbf{r})$, thus providing a route for analyzing, evaluate and classify the nature of chemical bonds and interactions.[39,40] The sound basis of the QTAIM analysis, from a chemist point of view, is that this approach (at least in its pure form) relies on an observable, which can be probed via X-ray diffraction experiments. It is worth noting that recently, some authors have studied the spin-dependent relativistic effects on the electron density, but only a crude analysis of the impact on the bonding pictures is reported.[41,42]

As a support for the originality of the proposed approach, illustrations of the SOC effects on the bond representation are given for selected astatine species. Astatine (At, $Z = 85$) is the heaviest naturally occurring halogen, traditionally located below iodine in the periodic table of the elements. One of its longest-lived isotopes, $^{211}$At, is of considerable interest in nuclear medicine as radiotherapeutic agent for targeted alpha therapy.[43,44] It has been highlighted recently that many basic chemical studies of At have unfortunately been set aside, which currently hinders the development of radiotherapeutic agents.[45] At isotopes are artificially produced in cyclotrons and due to their short half-life times (<8 h), all investigations were consequently derived from radiochemical studies at ultratrace concentrations (typically smaller than $10^{-10}$ mol $L^{-1}$). Therefore, no spectroscopic tools can be used to study At chemistry at the molecular scale. Theoretical methods thus represent a valuable tool to gain insights into the chemistry of this "invisible" element. It has been shown that numerous properties of At species are highly sensitive to SOC.[25,38,46−50] With the notable exception of HAt molecule,[11,12,51] no information can be retrieved from the literature regarding the nature of At-bonds in experimentally identified compounds. The present work aims also at filling this blank space through the coupled use of the QTAIM and ELF topological analyzes.

## 2. THEORY

**2.1. QTAIM Analyses.** This approach relies on the theory of gradient dynamical systems which enables a partitioning of the 3D molecular space into topological basins (namely electronic volumes) via the properties of the electron density gradient field.[40] As the electron density exhibits large maxima ($\nabla\rho(\mathbf{r}) = 0$) at the nuclear positions, QTAIM topological basins are only atomic, and thus, a topological atom A can be defined as the union of a nucleus and of its atomic basin. Atomic basins are delimited by zero-flux surfaces. The integration of the electron density over the atomic basins provides an atomic population. The atomic charge, $q(\mathrm{A})$, is calculated by subtracting the atomic population from the atomic number. In the context of the spin−orbit DFT (SODFT) method,[52] which is used in this work to perform quasirelativistic quantum calculations, $\rho(\mathbf{r})$ is obtained from 2c spinors, $\varphi_i(\mathbf{r})$. The latter are expanded using atom-centered Gaussian basis functions, $\chi_\mu(\mathbf{r})$:

$$\varphi_i(\mathbf{r}) = \begin{pmatrix} \varphi_{i\alpha}(\mathbf{r}) \\ \varphi_{i\beta}(\mathbf{r}) \end{pmatrix} = \begin{pmatrix} \sum_\mu c_{i\mu}^{\alpha}\chi_\mu(\mathbf{r}) \\ \sum_\mu c_{i\mu}^{\beta}\chi_\mu(\mathbf{r}) \end{pmatrix} \tag{1}$$

where the expansion coefficients, $c_i$, are complex. The total electron density is then defined as

$$\begin{aligned} \rho(\mathbf{r}) &= \sum_i^{\mathrm{occ}} \varphi_i^{\dagger}(\mathbf{r})\varphi_i(\mathbf{r}) \\ &= \sum_i^{\mathrm{occ}} (\varphi_{i\alpha}^{*}(\mathbf{r})\varphi_{i\alpha}(\mathbf{r}) + \varphi_{i\beta}^{*}(\mathbf{r})\varphi_{i\beta}(\mathbf{r})) \\ &= \sum_\mu \sum_\nu P_{\mu\nu}\chi_\mu(\mathbf{r})\chi_\nu(\mathbf{r}) \end{aligned} \tag{2}$$

where $P_{\mu\nu}$ are elements of the total density matrix:

$$P_{\mu\nu} = \sum_i^{\mathrm{occ}} (c_{i\mu}^{\alpha}(c_{i\nu}^{\alpha})^{*} + c_{i\mu}^{\beta}(c_{i\nu}^{\beta})^{*}) \tag{3}$$

Note that, due to the use of pseudopotentials (PPs) for some atoms, the calculation of their atomic charge involves $Z_{\mathrm{eff}}$, the charge of the inner-core, rather than the atomic number.

Beyond the population analysis, the molecular dipole moment, $\mu$, can be computed using the topological electrostatic distributed moments.[53] Note that this formalism has been extended to more complex topologies such as the one of ELF.[54] Within the QTAIM framework, the molecular dipole is calculated as the sum of the origin-dependent charge transfer contributions and the dipolar polarization contribution of the atomic basin:

$$\mu = \sum_{\mathrm{A}} (q(\mathrm{A})\mathbf{R}(\mathrm{A}) + \mathbf{M1}(\mathrm{A})) \tag{4}$$


dx.doi.org/10.1021/ct500762n | J. Chem. Theory Comput. 2014, 10, 4830−4841

where $q(A)$ is the total charge of the atomic basin, $\mathbf{R}(A)$ is the location of the A nucleus, and $\mathbf{M1}(A)$ is the dipolar moment vector of the A atom for which its components are expressed as follows:

$$M1_i(A) = -\int_A (i - R_i(A))\rho(\mathbf{r})\, d\mathbf{r} \quad i = x, y, z \tag{5}$$

If the charge density is isotropic around the atoms in the molecule, the dipolar moments $\mathbf{M1}(A)$ vectors will be zero, which is obviously never the case. Thus, nonzero values of topological moments indicate an anisotropy of the charge distribution in the topological basins.[55]

Overall, the critical points of the density gradient field are the points where $\nabla\rho(\mathbf{r}) = 0$. These points can be either local maxima (attractors), minima or saddle points of the gradient field. These points are usually single points, but exceptions can occur if the system belongs to a continuous symmetry group ($C_{\infty v}$ for instance). Among the saddle points, a *bond critical point* (BCP) is only connected to two maxima by the trajectories of the gradient field (bond path). The QTAIM theory predicts that the values of some local indicators calculated at the BCP are closely related to the nature of interactions between atoms. It is acknowledged that the density at the BCP, $\rho_b$, is in general larger than 0.20 e bohr$^{-3}$ in *shared-shell* interactions, in other words, covalent bonds, and smaller than 0.10 e bohr$^{-3}$ in *closed-shell* interactions (e.g., ionic, van der Waals, hydrogen bonding).[56] A sharper classification between these two type of bonding is achieved using indicators that rely on the local expression of the virial theorem:[40]

$$\frac{1}{4}\nabla^2\rho(\mathbf{r}) = 2G(\mathbf{r}) + V(\mathbf{r}) \tag{6}$$

Here, $\nabla^2\rho(\mathbf{r})$ is the Laplacian of the density, $G(\mathbf{r})$ is the positive definite kinetic energy density (also referred as $T_s(\mathbf{r})$ in the literature), and $V(\mathbf{r})$ is the potential energy density (negative). According to eq 6, we observe that if the Laplacian of the density at the BCP, $\nabla^2\rho_b$, is negative, the potential energy density ($V_b$) locally dominates (charge concentration), which indicates a shared-shell interaction. In contrast, if the kinetic energy density at the BCP ($G_b$) dominates, $\nabla^2\rho_b$ is positive (charge depletion) which characterizes closed-shell interactions.[57] Note that the energy densities at the BCP are extensively used as well to classify chemical bonds into shared-shell and closed-shell interactions. One can define the ratio $|V_b|/2G_b$, which is larger than 1 when $\nabla^2\rho_b < 0$, while it is smaller than 1 when $\nabla^2\rho_b > 0$. A second energetic descriptor is used to differentiate two categories of closed-shell bonding: the $|V_b|/G_b$ ratio that reflects the covalency magnitude of the interaction.[56,58] If the latter ratio is smaller than 1, the kinetic energy density is the leading term and electrons are destabilized close to the BCP, no covalency is expected (for example pure ionic or van der Waals bonding). The interactions are called *pure* closed-shell interactions (*pure* CS). The second category of closed-shell bonding, with some sharing of electrons ($|V_b|/G_b > 1$, i.e. the potential energy density is large and electrons are stabilized at the BCP), is called after Nakanishi et al.[59] *regular* closed-shell (*regular* CS). Thus, the analysis of the $\rho_b$, $\nabla^2\rho_b$, $V_b$, and $G_b$ values provide information about the bonding schemes, as illustrated in Scheme 1.

In the 2c relativistic formalism, the kinetic energy density and the Laplacian of the density are evaluated from the primitive functions $\chi_\mu$ and the density matrix elements $P_{\mu\nu}$:[38]

**Scheme 1. Typical QTAIM Classification of Interactions**

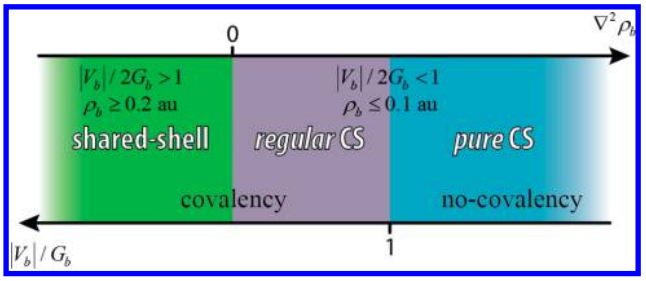


$$G(\mathbf{r}) = \frac{1}{2}\sum_\mu\sum_\nu P_{\mu\nu}\left(\frac{\partial\chi_\mu(\mathbf{r})}{\partial x}\frac{\partial\chi_\nu(\mathbf{r})}{\partial x} + \frac{\partial\chi_\mu(\mathbf{r})}{\partial y}\frac{\partial\chi_\nu(\mathbf{r})}{\partial y} + \frac{\partial\chi_\mu(\mathbf{r})}{\partial z}\frac{\partial\chi_\nu(\mathbf{r})}{\partial z}\right) \tag{7}$$

$$\nabla^2\rho(\mathbf{r}) = \sum_\mu\sum_\nu P_{\mu\nu}\left(\frac{\partial^2\chi_\mu(\mathbf{r})}{\partial x^2}\chi_\nu + \frac{\partial^2\chi_\nu(\mathbf{r})}{\partial x^2}\chi_\mu + \frac{\partial^2\chi_\mu(\mathbf{r})}{\partial y^2}\chi_\nu + \frac{\partial^2\chi_\nu(\mathbf{r})}{\partial y^2}\chi_\mu + \frac{\partial^2\chi_\mu(\mathbf{r})}{\partial z^2}\chi_\nu + \frac{\partial^2\chi_\nu(\mathbf{r})}{\partial z^2}\chi_\mu + 2\frac{\partial\chi_\mu(\mathbf{r})}{\partial x}\frac{\partial\chi_\nu(\mathbf{r})}{\partial x} + 2\frac{\partial\chi_\mu(\mathbf{r})}{\partial y}\frac{\partial\chi_\nu(\mathbf{r})}{\partial y} + 2\frac{\partial\chi_\mu(\mathbf{r})}{\partial z}\frac{\partial\chi_\nu(\mathbf{r})}{\partial z}\right) \tag{8}$$

The potential energy density is then readily obtained by differentiation using eq 6.

**2.2. ELF Topological Analyzes.** ELF has been recently extended to the 2c relativistic formalism, and the reader can find in ref 38 a complete description of this aspect. In a similar way as the QTAIM topological analysis, presented in the previous section, the topological analysis of ELF leads to a partitioning of the 3D molecular space into volumes, the ELF basins.[35] ELF tends to 1 in the regions where electronic pairs are strongly localized and to zero at the boundaries between such regions. Each ELF basin has a chemical significance, for instance core basins labeled C(A), around nuclei A, and valence basins. The latter are split in nonbonding basins, labeled V(A), that usually correspond to lone pair regions, and bonding basins, labeled V($A_i$, $A_j$), that characterize the covalent bonds between two A atoms. The integration of the electron density over the volumes of basins provides average basin populations. The basin populations should be understood as arising from Lewis resonant structures and it is possible to calculate some weights of these formal Lewis structures.[60,61] Moreover, a statistical analysis of basin populations enables one, through the definitions of the variance and the covariance matrix, to obtain information about the electron delocalization between basins.[61,62] Indeed, the variance for a given basin (noted $\sigma^2$) is interpreted as a measure of the electron density fluctuation with all the other basins, while the values of the covariance matrix elements are a measure of the correlation between the populations of two given basins. These statistical quantities are very useful for characterizing some particular bonding schemes, such as the charge-shift bonding for which the dynamical


dx.doi.org/10.1021/ct500762n | J. Chem. Theory Comput. 2014, 10, 4830−4841

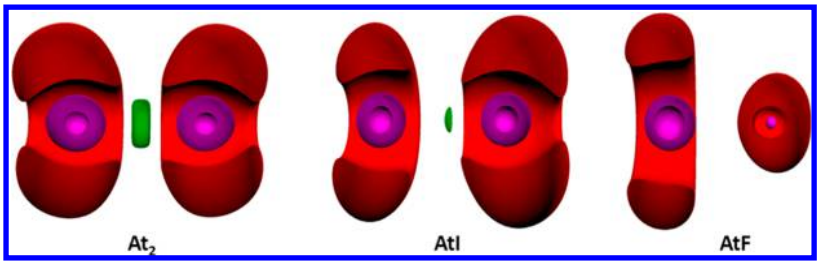


**Figure 1.** Split of ELF localization domains (isosurface = 0.7) of the AtX species (X = At, I, F) calculated at the 2c-B3LYP/aug-cc-pVTZ-PP-2c level of theory. Color code: magenta for core C(X) basins, red for valence V(X) basins, and green for bonding V(At, X) basins.

delocalization of populations between lone pair basins is a typical signature.[62]

**2.3. Computational Details.** The SODFT method implemented in the NWChem programs package[52] has been successfully used to investigate SOC effects on molecules containing At.[25,38,46,63−65] Details of this 2c approach can be found in ref 38 and references therein. Geometry optimizations at the SODFT level of theory have been carried out prior to the topological analyzes. Harmonic vibrational frequencies were evaluated by two sided finite differences of analytical gradients. The small-core ECP*n*MDF PPs with $n$ = 10, 28, and 60 have been used for the Br, I, and At atoms, respectively.[66,67] For describing the remaining 25 electrons of these atoms, we have opted for the aug-cc-pVTZ-PP basis set[66] for Br, the aug-cc-pVTZ-PP-2c basis set[68] for At, and the one assembled from the aug-cc-pVTZ-PP basis set[67] and 2c extensions[69] for I. The aug-cc-pVTZ basis set[70−72] was used for the lighter atoms, H, B, C, N, O, F, and Cl. The applied density-functional approximation was the widely used B3LYP hybrid functional.[73] The reliability of the B3LYP functional for the study of At species has been investigated previously.[38,46,63−65,74,75]

In order to evaluate SOC effects on the studied species, geometry optimizations and frequency calculations have also been done at a scalar relativistic level through DFT calculations, in the absence of spin-dependent potentials in PPs. Afterward, new QTAIM and ELF topological analyzes have been carried out.

Note that in all the cases, the studied species are oriented such that the At-bonds are along the $z$-axis. All the topological analyses here presented have been carried out using modified versions of the NWChem[52] and TopMoD09[76] program packages. The relevant program files which implement the treatment of 2c wave functions are freely available upon request. Isosurfaces have been drawn using either Molekel[77] or GaussView[78] programs.

## 3. RESULTS AND DISCUSSION

**3.1. $At_2$ Species.** Our objective is to investigate, by means of topological tools, how the At-bond is affected by SOC. Indeed, SOC effects are recognized to strongly affect At properties.[25,38,46−49] The $At_2$ species represents an invaluable illustration and deserves a special attention: it has been the subject of numerous theoretical studies. For instance, it comes out that the stretching frequency ($\omega_e$) is reduced by almost 50% by SOC and the (negative) SOC contribution to the dissociation energy ($D_e$) is greater than $D_e$ itself.[46,75,79] Using the topological analysis of the ELF function, some of us have previously investigated the weakening of the $At_2$ bond induced by SOC.[38] Figure 1 displays the ELF localization domains determined for $At_2$ while the electron populations of the ELF basins are recalled in Table 1. A strong decrease of the

**Table 1. ELF Electron Population Analysis and QTAIM Properties of the $At_2$ Species at the 2c-B3LYP/aug-cc-pVTZ-PP-2c Level of Theory**

| ELF | core | valence | | |
|---|---|---|---|---|
| | C(At) | V(At) | pop $\pi^b$ | V(At, At) |
| | 17.77 | 6.96 | 7.66 | 0.54 |
| ΔSO[a] | +0.02 | +0.16 | +1.52 | −0.36 |
| QTAIM | at the bond critical point | | | |
| | $\rho_b \times 10^{2c}$ | $\nabla^2\rho_b \times 10^{2d}$ | $\lvert V_b\rvert/G_b$ | $\lvert V_b\rvert/2G_b$ |
| | 4.6 | 3.0 | 1.54 | 0.77 |
| ΔSO[a] | −1.5 | +0.8 | −0.21 | −0.11 |

[a]The spin−orbit effects are defined as the difference between quasirelativistic and scalar-relativistic computed values. [b]The $\pi$ population of both V(A) valence basins is evaluated by only taking into account the expansion coefficients of the $p_x$ and $p_y$ Gaussian basis functions during the integration of the electron density over the basin volumes. [c]Electron density (e bohr$^{-3}$). [d]Laplacian of the electron density (e bohr$^{-5}$).

population of the V(At, At) bonding basin in favor of the valence V(At) nonbonding basins was demonstrated. This SOC effect has been rationalized as an electron withdrawal from the covalent $\sigma$ bond to the valence $\pi$ system, which is essentially located in the lone pair regions, in agreement with previous analyzes done in term of molecular spinors.[10,75]

Although the topological representation offers a rather satisfactory interpretation of the bonding, phenomenological descriptions in terms of Lewis resonant structures are often very helpful, at least, as explanatory models. In the case of $At_2$, the bonding could be rationalized using the Pauling's classical paradigm[80] based on the superposition of a covalent form, $:\ddot{A}t-\ddot{A}t:$ (**1**), stabilized by electron pair sharing, and two ionic forms, $^{\oplus}:\ddot{A}t\ \ :\ddot{A}t:^{\ominus}$ (**2**) and $^{\ominus}:\ddot{A}t:\ \ \ddot{A}t:^{\oplus}$ (**3**), resulting from the static charge distribution in the molecule. This implies that the electronic population of the ELF basins should be understood as arising from the three Lewis resonant structures.[60,61] Hence, the covalent and the two ionic structures are roughly weighted with values $w_1$ = 0.26 and $w_2$ = $w_3$ = 0.37, respectively. According to what was found for the other homonuclear dihalogens (see ref 62 and Table S1 in the Supporting Information), the electron pair sharing in the covalent structure brings a small contribution to the bonding since a small electron density in the bonding region is found. The leading contribution of the ionic structures is confusing for a homonuclear bond, where static charge distributions should be unimportant. The classical Pauling scheme appears inappropriate for $At_2$ species. Recently another class of bonding has emerged, the charge-shift (CS) bonding,[81] where significant fluctuations of the electron pair density results from ionic−


dx.doi.org/10.1021/ct500762n | J. Chem. Theory Comput. 2014, 10, 4830−4841

Table 2. ELF Electron Population Analysis of AtX Species (X = I, Br, Cl, F, H) Obtained at the 2c-B3LYP/aug-cc-pVTZ-PP-2c Level of Theory

| | core | | | valence | | |
|---|---|---|---|---|---|---|
| basins | C(At) | C(X) | V(At) | V(X) | pop $\pi^b$ | V(At, X) |
| AtI | 18.06 | 17.70 | 6.43 | 7.09 | 7.02 | 0.68 |
| $\Delta SO^a$ | +0.01 | +0.01 | +0.05 | +0.19 | +1.14 | −0.26 |
| AtBr | 18.06 | 17.87 | 6.39 | 7.12 | 7.53 | 0.56 |
| $\Delta SO^a$ | +0.01 | +0.01 | +0.02 | +0.21 | +1.91 | −0.25 |
| AtCl | 18.33 | 10.04 | 5.97 | 7.02 | 6.58 | 0.63 |
| $\Delta SO^a$ | +0.03 | 0.00 | −0.12 | +0.16 | +0.54 | −0.08 |
| AtF | 18.53 | 2.18 | 5.83 | 7.46 | 6.66 | c |
| $\Delta SO^a$ | +0.01 | 0.00 | −0.04 | +0.03 | +0.39 | c |
| AtH | 17.46 | c | 6.71 | c | 4.02 | 1.83 |
| $\Delta SO^a$ | +0.02 | c | +0.02 | c | +0.61 | −0.04 |

[a]The spin−orbit effects are defined as the difference between quasirelativistic and scalar-relativistic computed values. [b]The $\pi$ population of the valence basins V(A) + V(X) is evaluated by only taking into account the expansion coefficients of the $p_x$ and $p_y$ Gaussian basis functions during the integration of the electron density over the basin volumes. [c]No ELF basin of this type was found.

Table 3. QTAIM Properties of AtX Species (X = I, Br, Cl, F, H) Obtained at the 2c-B3LYP/aug-cc-pVTZ-PP-2c Level of Theory

| | integrated properties | | at the bond critical point | | | |
|---|---|---|---|---|---|---|
| | $q$(At)$^b$ | $\mu^c$ | $\rho_b \times 10^{2d}$ | $\nabla^2\rho_b \times 10^{2e}$ | $\lvert V_b\rvert/G_b$ | $\lvert V_b\rvert/2G_b$ |
| AtI | 0.19 | 1.58 | 5.7 | 3.0 | 1.65 | 0.82 |
| $\Delta SO^a$ | +0.10 | +0.96 | −0.9 | +1.1 | −0.16 | −0.08 |
| AtBr | 0.31 | 2.30 | 6.7 | 5.6 | 1.56 | 0.78 |
| $\Delta SO^a$ | +0.06 | +1.03 | −1.0 | +1.1 | −0.12 | −0.06 |
| AtCl | 0.45 | 2.80 | 7.6 | 8.7 | 1.51 | 0.75 |
| $\Delta SO^a$ | +0.09 | +0.96 | −1.2 | +0.6 | −0.09 | −0.05 |
| AtF | 0.64 | 3.26 | 10.6 | 33.8 | 1.28 | 0.64 |
| $\Delta SO^a$ | +0.03 | +0.70 | −1.2 | +4.2 | −0.03 | −0.01 |
| AtH | 0.12 | 0.21 | 12.8 | −4.4 | 2.17 | 1.09 |
| $\Delta SO^a$ | +0.01 | +0.26 | −0.9 | +1.7 | −0.05 | −0.02 |

[a]The spin−orbit effects are defined as the difference between quasirelativistic and scalar-relativistic computed values. [b]At atomic charge (e). [c]Molecular dipole moment (D). [d]Electron density (e bohr$^{-3}$). [e]Laplacian of the electron density (e bohr$^{-5}$).

covalent mixing. In other words, CS bonds are more related to the dynamic bond ionicity (a significant quantity of electronic density fluctuates back and forth from one atom to the other) rather than electrostatic interactions between static charge distributions. The CS bonding territory involves notably homopolar bonds of compact electronegative and/or lone pair-rich elements, and heteropolar bonds of these elements. The CS bonding rules the chemical bond in the $F_2$, $Cl_2$, and $Br_2$ molecules[62,81] and is thus expected to greatly contribute to the bond cohesion in $At_2$. Indeed, $At_2$ exhibits one of the most depleted bonding basins (i.e., weak covalency) among the dihalogens (see Table S1 in the Supporting Information). Further original insights in the At-bonds can be obtained from comparison of the results of relativistic calculations with and without SOC included. The difference defines the SOC effects (ΔSO), manifested in Table 1 by a 40% decrease of the electron population of the V(At, At) bonding basin in favor of the V(At) valence basins. This can be rationalized as the SOC increases the electron density in the lone pair regions and the At propensity to make CS bonds, while it lowers in the same time the covalent bonding. The latter behavior is also revealed by the QTAIM topological analysis.

Some properties of the electron density computed at the BCP are presented in Table 1. $\rho_b$ is notably weak, 0.05 e bohr$^{-3}$, and lowered by the SOC (ΔSO = −0.01 e bohr$^{-3}$). Such a low $\rho_b$ value is commonly associated with closed-shell interactions (for example ionic, van der Waals, hydrogen bonding, etc.).[56] For the studied case, which cannot possess static bond-ionicities, the computed value of $\rho_b$ is obviously not related to ionic bonding. Considering the small positive $\nabla^2\rho_b$ value, $At_2$ definitively does not fit the shared-shell category (dominant covalent bonding) but obviously its homopolar bond cannot be classified as ionic (large positive $\nabla^2\rho_b$ value). Similarly, it has been established for other species dominated by CS bonding that they do not satisfy the standard QTAIM classification.[81,82] Two signatures of CS bonding emerge for homonuclear diatomics: depleted electron density at midbond and a small negative or positive $\nabla^2\rho_b$ value. This is consistent with the values reported in Table 1 for the $At_2$ species. Note that the calculated value of the $|V_b|/2G_b$ ratio, 0.77 (see Table 1), is consistent with the small positive $\nabla^2\rho_b$ value, testifying for some kind of closed-shell interactions. The $|V_b|/G_b$ ratio informs us about the covalency magnitude in $At_2$. Since $|V_b|/G_b$ = 1.54, some sharing of electrons is expected and the interaction between both At atoms does not fit the *pure* CS category. It is worth noting that the SOC markedly lower the weight of covalency (ΔSO = −0.22). Briefly, the QTAIM topology analysis (i) reveals a depleted electron density at midbond and a small positive $\nabla^2\rho_b$ value, which are recognized features of CS bonding, (ii) shows that the relativistic SOC weakens the magnitude of the covalent interaction, and (iii) discards ionic or weak (like van der Waals bonding) closed-shell interactions.

**3.2. Heteronuclear Dihalogens.** We now continue this work with AtX dihalogens (X = I, Br, Cl, F) in order to investigate the combination of SOC and electronegativity effects on At-bonds. Furthermore, AtI, AtBr, and AtCl are among the few At compounds that have been studied experimentally[46,83,84] and that have recently attracted the attention of theoretical chemists.[46,85] Figure 1 displays the ELF localization domains determined for the AtI molecule. The same typical topologies have been found for AtBr and AtCl molecules: two core basins, C(At) and C(X), two valence basins, V(At) and V(X), accounting for nonbonding density, and one bonding basin, V(At, X). The basin populations of these species are presented in Table 2. The topological properties of the bonding basin V(At, X) deserve special attention as they are crucial to evaluate how much the covalent character is affected by SOC effects. As previously found for $At_2$ species, the population of the bonding basin for AtI (0.68 e), AtBr (0.56 e), and AtCl (0.63 e) molecules is weak. It indicates that the bonds in AtI, AtBr, and AtCl are not classical covalent bonds (a bonding population of two electrons is expected for a purely covalent single bond). One can notice that SOC decreases notably the population of the bonding basin. For example, the V(At, I) population in AtI molecule changes from 0.94e to 0.68e when spin-dependent effects are taken into account. The electron population drop varies in the following order: $At_2$, AtI, AtBr, and AtCl. From the QTAIM topological analyzes and the reported values in Table 3, it comes out also


dx.doi.org/10.1021/ct500762n | J. Chem. Theory Comput. 2014, 10, 4830−4841

**Table 4. Spectroscopic Constants of AtX Species (X = At, I, Br, Cl, F, H) Obtained at the 2c-B3LYP/aug-cc-pVTZ-PP-2c Level of Theory**

| | $R_e$ (Å) | $\omega_e$ (cm$^{-1}$) | $k$ (N m$^{-1}$) |
|---|---|---|---|
| $At_2$ | 3.048 | 109 | 73 |
| ΔSO[a] | +0.167 | −44 | −72 |
| AtI | 2.879 | 153 | 110 |
| ΔSO[a] | +0.085 | −30 | −47 |
| AtBr | 2.671 | 201 | 137 |
| ΔSO[a] | +0.075 | −32 | −47 |
| AtCl | 2.524 | 298 | 157 |
| ΔSO[a] | +0.075 | −49 | −55 |
| AtF | 2.086 | 497 | 254 |
| ΔSO[a] | +0.058 | −70 | −76 |
| AtH | 1.741 | 1981 | 232 |
| ΔSO[a] | +0.031 | −196 | −48 |

[a]The spin−orbit effects are defined as the difference between quasirelativistic and scalar-relativistic computed values.

that SOC lowers the $|V_b|/G_b$ ratio which reflects the magnitude of covalency (see ΔSO values). The fact that SOC decreases the electron pair sharing in At-bonds was previously associated with the weakening of the bond strength in the $At_2$ species.[38] As shown in Table 4, this is also the case for the AtI, AtBr, and AtCl molecules as the bond distances ($R_e$) increase due to the SOC while the stretching frequencies ($\omega_e$) are lowered. Since the force constant $k$ is not biased by atomic masses, it is a better probe than the stretching frequency for comparing the bond strengths of different species. The inclusion of SOC in the DFT calculations reduces $k$ by 50% for $At_2$, 30% for AtI, and 26% for AtBr and AtCl.

While the SOC decreases the population of the V(At, X) bonding basins, the results in Table 2 show an increase for the valence nonbonding basins. Due to electronegativity differences between the At and X atoms (At is thought to have an electronegativity of 2.2 on the revised Pauling scale),[86] the electron population growth is more pronounced for the V(X) basins than for V(At). In the case of AtCl and AtF molecules, the growth of V(Cl) and V(F) populations originates mainly from the decrease of the V(At) population. The redistribution of the electron density, due to the SOC, appears to be influenced by the electronegativity of the involved elements. The atomic charges determined from the QTAIM analysis are even more informative. Indeed, as can be seen in Table 3 for the AtI, AtBr, AtCl, and AtF species, the SOC systematically induces a rise of the positive At charge, $q$(At). For example, the $q$(At) value in AtI changes from +0.09e to +0.19e. The SOC effectively enlarge the electronegativity differences between the At and X atoms. This behavior is also illustrated by the change of the molecular dipole moment values (see Table 3). The latter are increased by about +1 D for AtI, AtBr, and AtCl, and +0.7 D for AtF. As the effects of SOC are expected to be more pronounced for At than for any other halogen, we conclude that SOC markedly decreases the effective At electronegativity in molecules.

Among the AtX dihalogens (X = At, I, Br, Cl, F), the AtF species is the least affected by SOC. Note that it also exhibits the strongest bond, witnessed by a force constant of 254 N m$^{-1}$ (see Table 4). Figure 1 displays the ELF localization domains determined for AtF. The topology does not exhibit a bonding basin, which is typical for essentially ionic bonds. This is consistent with the calculated QTAIM descriptors (see Table 3): (i) the low value of $\rho_b$, 0.11 e bohr$^{-3}$, and (ii) the large positive value of $\nabla^2\rho_b$, 0.34 e bohr$^{-5}$, are representative of mainly ionic bonds. Nevertheless, the $|V_b|/G_b$ ratio is larger than 1 and discloses some covalency. Following the QTAIM approach, the bonding in AtF falls in the *regular* CS category. The situation is less clear for the AtI, AtBr, and AtCl molecules. In this cases, similar $\rho_b$ (about 0.07 e bohr$^{-3}$) and $\nabla^2\rho_b$ (about 0.06 e bohr$^{-5}$) values have been found, which are closer to the ones obtained for the $At_2$ species rather than the ones obtained for AtF. Other similar bonding properties exist between the $At_2$ and the AtI, AtBr, and AtCl molecules. All have weakly populated ELF bonding basins (less than 1 e) and the variances $\sigma^2$ of these populations are large. This indicates a significant charge density fluctuation of the bonding electrons. For AtCl, the variance calculated from scalar-relativistic computations represents 83% of the total V(At, Cl) population, in close agreement with what was found for $At_2$ (see Table S2 in the Supporting Information). Furthermore, a large negative covariance matrix element, $\langle \mathrm{cov(At, Cl)} \rangle = -0.32$ e, has been found for AtCl between the valence nonbonding basins, which means that a significant quantity of electronic density fluctuates back and forth from one atom to the other. A depleted bonding basin population with a large variance and negative covariance are typical manifestations of CS bonding.[62] Indeed, the fact that CS bonding plays some role in AtCl, AtBr, and AtI molecules cannot be ruled out. It has been rationalized that CS bond originates primarily from the repulsion between the bonding electrons and the lone pairs, adjacent to the bond, that have the same symmetry ($\sigma$ in dihalogen molecules).[62,81] This effect weakens the covalent contribution to the bonding, referred to as the lone pair bond-weakening effect (LPBWE),[87] and the bond stabilization is achieved by the covalent-ionic fluctuation of the electron pair density. Interestingly, the comparison between the ELF topologies obtained from the 2c and scalar-relativistic calculations, shown in Table 2 for AtCl, AtBr, and AtI molecules (see ΔSO values) and previously discussed for $At_2$,[38] shows that the SOC markedly increases the $\pi$ population of the valence nonbonding basins while the total population of the bonding basins decreases at the same time. It shall be regarded as an electron withdrawal from the covalent $\sigma$ bond to the valence $\pi$ system that is essentially located in the lone pair regions. This behavior is clearly in line with the LPBWE and obviously demonstrates that the CS bonding goes along with the SOC interaction.

The AtH molecule has been included in this section since the H atom shares some features with halogens (it was sometimes placed on top of the 17th column in the periodic table), and At is thought to have an electronegativity matching the one of H.[86] Hence, the H atom can be used to probe features of $\sigma$-bonding in At-bonds, and especially the combination of SOC and electronegativity effects. Saue et al.[12] performed on AtH relativistic Hartree−Fock calculations based on the Dirac−Coulomb (DC) Hamiltonian. They argued for covalent bonding in view of the calculated dipole moment, 0.06 D with the negative charge on the H atom. The spectroscopic constants have been determined by Gomes et al.[88] using relativistic coupled cluster DC−CCSD(T) calculations with flexible triple-$\zeta$ basis sets. The best reported values for $R_e$ and $\omega_e$, 1.718 Å and 1992 cm$^{-1}$, respectively, are fairly close to ours (1.741 Å and 1981 cm$^{-1}$ in Table 4). SOC effects were found to weaken the AtH bond, enlarging $R_e$ by +0.029 Å and reducing $\omega_e$ by −215 cm$^{-1}$ (our calculations yield similar results, +0.031 Å and −196 cm$^{-1}$ respectively). The classic


dx.doi.org/10.1021/ct500762n | J. Chem. Theory Comput. 2014, 10, 4830−4841

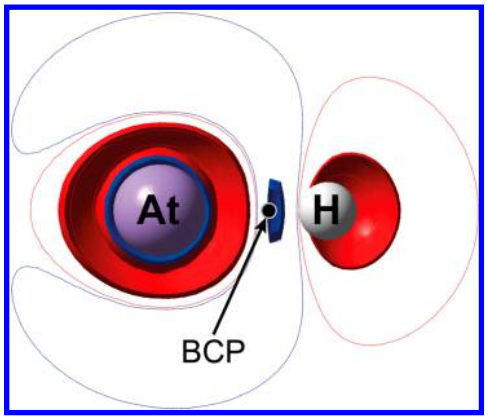


**Figure 2.** Difference between the quasirelativistic and scalar-relativistic electronic densities of the AtH molecule at the equilibrium distance of 2c-B3LYP/aug-cc-pVTZ-PP-2c calculations. The surfaces (isovalue = 0.001 e bohr$^{-3}$) in red color show the area where the difference is very positive and in blue color the area where the difference is very negative. A spacing of 0.0001 e bohr$^{-3}$ is used for the contour plots.

explanation is that SOC mixes antibonding $\sigma$ character into the nonbonding $\pi$ orbitals (representing At lone pairs in the nonrelativistic limit), which weakens the bond.[11] Using the scalar-relativistic Douglas−Kroll Hamiltonian and the relativistic DC Hamiltonian, Norman et al.[89] showed at the Hartree−Fock level that SOC is able to invert the dipole moment orientation. Previously,[90] Dolg estimated the dipole moment to 0.19 ± 0.05 D (the polarity of AtH being $At^{\delta+}H^{\delta-}$), on the basis of scalar multireference average coupled-pair functional (ACPF) calculations with additional SOC contributions from 2c Kramers-restricted CISD calculations. The present QTAIM analysis leads to consistent values of dipole moment, 0.21 D, and At atomic charge, +0.12 e. Let us consider the other QTAIM indicators presented in Table 3. The $\rho_b$ value, 0.13 e bohr$^{-3}$, and the negative $\nabla^2\rho_b$ value, −0.05 e bohr$^{-5}$, are representative of shared-shell interactions. The covalent nature of AtH is also witnessed by the large value of the $|V_b|/G_b$ ratio, 2.17. This is in line with the ELF analysis. The ELF topology exhibits three localization domains corresponding to one core basin and one valence nonbonding basin, both belonging to At, and one protonated basin, V(At, H). The latter accounts for the shared electron pair and its population, 1.83 e in Table 2, is close to the two electrons expected for a purely covalent single bond.

The SOC effects on both the ELF and the QTAIM topologies seem rather limited. The most striking effect is the change of the molecular dipole moment, from −0.05 D to +0.21 D (see Table 3). This can be rationalized as follows: in scalar-relativistic calculations, the bonding in AtH is mainly due to the overlapping between one At 6p orbital and the H 1s orbital. With SOC, the 6p orbitals are split into $6p_{1/2}$ and $6p_{3/2}$ atomic spinors, the latter being destabilized (energy rise) and become more diffuse (displacement of their radial maxima). AtH was found to be dominated by $6p_{3/2}$ bonding,[12,51] which thus leads to a bond lengthening with respect to scalar-relativistic results. Furthermore, rather than the single 1s electron of H completing the At valence p shell, the electron flow is more likely in the other way, with a raised $6p_{3/2}$ donating into the H 1s orbital. It is manifested by the reversed orientation of the dipole moment, but actually not through the calculated atomic charges. Indeed, a trifling variation of $q$(At) is observed upon SOC ($\Delta$SO = +0.01 e, see Table 3) that does not reflect the lowering of the effective At electronegativity and the change of the dipole moment. This finding was also verified using atomic charges derived from either Mulliken or natural population (NPA) analyses. Figure 2 displays the modification of the electronic density upon SOC, demonstrating a net increase of $\rho$ on the H atom (see the large red colored surface enclosing the H atom) due to the lowering of At electronegativity. A decrease in the electron density is also apparent at the BCP (see the blue colored surface). Regarding the ELF topological analysis, the slight population decrease of the V(At, H) bonding basin can be understood in terms of two opposite effects. As discussed for the other At-species, the SOC induce an electron withdrawal from the covalent $\sigma$ bond to the valence $\pi$ system located in the lone pairs region (witnessed by the $\pi$ population increase of V(At) basin, see Table 2). The opposing effect, mentioned above, is the electron flow from the high-lying $6p_{3/2}$ spinor of At to the H 1s orbital.

**3.3. Bonding with Second Row Elements.** Shortly after its discovery in 1940,[91] the potential use of At for the therapy of human diseases has attracted strong attention.[92] The broad application of $^{211}$At in nuclear medicine, and more precisely in oncology, will require its attachment to disease-targeting carrier molecules. In this field, the general approach consists in using bifunctional reagents. One function is used to bind At while the other is conjugated to a biological vector (peptides, proteins, antibodies, ...). Despite the significant number of studies dedicated to the synthesis of efficient bifunctional reagents for

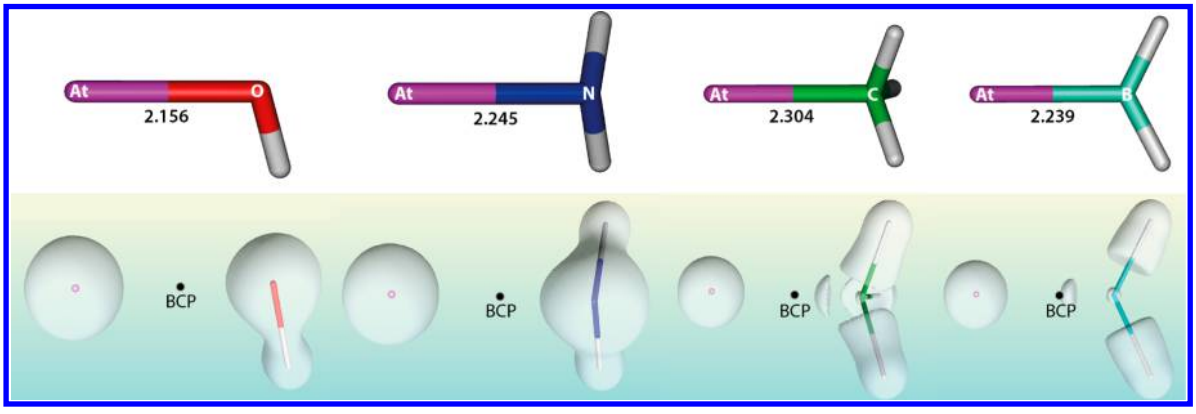


**Figure 3.** Calculated structures (top, distances in angstroms) and isosurfaces of the Laplacian of the electron density (bottom, $\nabla^2\rho$ = −0.02 e bohr$^{-5}$) for $AtXH_n$ species (X = O, N, C, B, $n$ = 1, 2, 3) at the 2c-B3LYP/aug-cc-pVTZ-PP-2c level of theory.

Table 5. ELF Electron Population Analysis of $AtXH_n$ Species (X = O, N, C, B, n = 1, 2, 3) Obtained at the 2c-B3LYP/aug-cc-pVTZ-PP-2c Level of Theory

| | core | | valence | | | |
|---|---|---|---|---|---|---|
| basins | C(At) | C(X) | V(At) | V(X) | V(At, X) | V(X, H) |
| AtOH | 18.74 | 2.13 | 5.74 | 2×(2.88) | *b* | 1.65 |
| ΔSO[a] | +0.02 | 0.00 | −0.02 | 2×(+0.05) | *b* | −0.04 |
| $AtNH_2$ | 18.08 | 2.11 | 6.43 | 3.29 | *b* | 2×(2.04) |
| ΔSO[a] | +0.02 | 0.00 | −0.01 | −0.12 | *b* | 2×(+0.05) |
| $AtCH_3$ | 17.69 | 2.09 | 7.56 | *b* | 0.42 | 3×(2.08) |
| ΔSO[a] | +0.03 | −0.01 | +0.74 | *b* | −0.82 | 3×(+0.02) |
| $AtBH_2$ | 17.33 | 2.06 | 6.77 | *b* | 1.72 | 2×(2.06) |
| ΔSO[a] | +0.03 | 0.00 | −0.06 | *b* | −0.01 | 2×(+0.02) |

[a]The spin−orbit effects are defined as the difference between quasirelativistic and scalar-relativistic computed values. [b]No ELF basin of this type was found.

Table 6. QTAIM Properties of $AtXH_n$ Species (X = O, N, C, B, *n* = 1, 2, 3) Obtained at the 2c-B3LYP/aug-cc-pVTZ-PP-2c Level of Theory

| | integrated properties | | | at the bond critical point | | | |
|---|---|---|---|---|---|---|---|
| | $q(At)^b$ | $q(X)^b$ | $\mu^c$ | $\rho_b \times 10^{2d}$ | $\nabla^2\rho_b \times 10^{2e}$ | $\lvert V_b\rvert/G_b$ | $\lvert V_b\rvert/2G_b$ |
| AtOH | 0.49 | −1.06 | 2.03 | 10.3 | 21.1 | 1.41 | 0.71 |
| ΔSO[a] | +0.03 | −0.02 | 0.63 | −1.2 | −1.3 | −0.04 | −0.02 |
| $AtNH_2$ | 0.40 | −1.12 | 1.33 | 9.7 | 9.7 | 1.60 | 0.80 |
| ΔSO[a] | +0.03 | 0.00 | 0.48 | −0.9 | +0.6 | −0.06 | −0.03 |
| $AtCH_3$ | 0.12 | −0.30 | 1.08 | 9.4 | 1.1 | 1.93 | 0.96 |
| ΔSO[a] | −0.01 | 0.00 | −0.34 | −0.7 | +11.2 | −0.09 | −0.04 |
| $AtBH_2$ | −0.06 | 1.29 | 0.06 | 10.2 | −11.5 | 3.04 | 1.52 |
| ΔSO[a] | +0.05 | −0.04 | −0.20 | −0.4 | +2.2 | −0.20 | −0.10 |

[a]The spin−orbit effects are defined as the difference between quasirelativistic and scalar-relativistic computed values. [b]Atomic charge (e). [c]Molecular dipole moment (D). Note that ΔSO values are unsigned if quasirelativistic and scalar-relativistic dipole moments are not collinear. [d]Electron density (e $bohr^{-3}$). [e]Laplacian of the electron density (e $bohr^{-5}$).

At-labeling, the in vivo stability of the current $^{211}$At-labeled organic compounds is so far unsatisfactory to be used in systemically targeted therapy of cancers.[43,44] Recently, it has been reported that the lack of knowledge on the basic chemistry of At hinders the development of innovative radiotherapeutic agents.[45] It is of indisputable interest to characterize the bonding between At and the usual elements used in organic chemistry to help rationalizing the already reported information and to further design new efficient bifunctional reagents. As a first attempt, At-bonds have been scrutinized for simple model compounds involving B, C, N and O elements: At−$BH_2$, At−$CH_3$, At−$NH_2$, and At−OH. While identified in gas phase by mass spectrometry almost half a century ago,[84] no published theoretical results are dedicated to the $AtCH_3$ molecule. Recently, Alkorta et al.[93] have theoretically evaluated the ability of AtOH species to make hydrogen bonds or halogen bonds with nitrogenated Lewis bases. However, the relativistic spin-dependent effects were not considered in their computations. The calculated structures of AtOH, $AtNH_2$, $AtCH_3$, and $AtBH_2$ species are displayed in Figure 3.

The results of the ELF and QTAIM topological analyses are presented in Tables 5 and 6. Regarding At-bonds in the AtOH and $AtNH_2$ species, some similarities can be noticed with AtF. On one hand, the ELF analysis shows no bonding basin between At and the heteroelement (X). This is usual for mainly ionic bonds. Consistently, the representation of the negative part of $\nabla^2\rho$ in Figure 3 shows no regions of local electronic charge concentration (isosurface with $\nabla^2\rho < 0$) between the At and X atoms. The $q$(At) and $q$(X) atomic charges also supplied by the QTAIM analysis are large and of opposite signs (see Table 6). It is worth noting that $q$(At) decreases regularly as X becomes less electronegative. On the other hand, the $\rho_b$ values (about 0.10 e $bohr^{-3}$) and the positive $\nabla^2\rho_b$ values (at least 0.10 e $bohr^{-5}$) obtained for the AtOH and $AtNH_2$ species, as for AtF, are consistent with mainly ionic bonds. Since the $|V_b|/G_b$ ratio is larger than 1, some covalency is also expected. In the QTAIM framework, the bonding in AtOH and $AtNH_2$ corresponds to the *regular* CS category. The properties displayed in Tables 5 and 6 are not much modified by the SOC, while At−O and At−N bond lengths are enlarged by about 0.05 Å. The latter observation is probably related to some weakening of both bonds.

The characterization of the At-bond in the $AtCH_3$ molecule is less clear cut. As for the $At_2$ species, the population of the ELF bonding basin is weak, 0.42 e (see Table 5), and it is decreased by 66% by SOC. Obviously, it cannot correspond to a purely covalent bond. The standard QTAIM classification fails also to characterize the bonding in $AtCH_3$: the SOC is by itself able to weaken the $\nabla^2\rho_b$ probe regarding the At-bond. While the scalar-relativistic DFT calculation leads to a negative $\nabla^2\rho_b$ value, −0.10 e $bohr^{-5}$, the analysis of the electronic density obtained from the SODFT calculation produces a trifling positive $\nabla^2\rho_b$ value, 0.01 e $bohr^{-5}$. Therefore, SOC brings this bond out of the shared-shell category (dominant covalent character) but does not allow the bond to be characterized by ubiquitous closed-shell interactions. Furthermore, at the same time as SOC decreases the population of the V(At, C) bonding basins, by −0.82 e, it increases by +0.74 e the population of the At valence nonbonding basins, V(At), which


dx.doi.org/10.1021/ct500762n | J. Chem. Theory Comput. 2014, 10, 4830−4841

stands for the At lone pairs (see Table 5). A closer inspection reveals that the V(At) population growth follows essentially the +0.67 e increase of the electron population described by the p Gaussian basis functions that are perpendicular to the At−C bond. Similarly to the $At_2$ case, SOC leads to an electron withdrawal from the covalent $\sigma$ bond in favor of the At lone pairs mainly perpendicular to the bond. It shall be regarded as a mark of the CS bonding that lowers the LPBWE, i.e. the repulsion between the $\sigma$ lone pair of the At atom and the $\sigma$ bonding electrons. The magnitude of the SOC effects in $AtCH_3$ molecule mirrors the increasing role played by the CS bonding in the At−C bond.

For the $AtBH_2$ species, the At-bond seems to be essentially covalent as in the AtH molecule. This is shown in Tables 5 and 6 by (i) the population of the corresponding V(At, B) bonding basin which is about 1.72 e (not far from 2 e) and (ii) the related $\rho_b$ and $\nabla^2\rho_b$ values, being respectively 0.10 e bohr$^{-3}$ and −0.12 e bohr$^{-5}$. The latter are representative of shared-shell interactions in the QTAIM classification. The covalent nature of the At-bond is also witnessed by the large value of the $|V_b|/G_b$ ratio, 3.04, and a region of local electronic charge concentration (isosurface with $\nabla^2\rho < 0$) that is displayed in Figure 3 close to the BCP. The most interesting outcome disclosed by the QTAIM topological analysis is the negative charge of the At atom, −0.06 e. This reflects the greater electronegativity of At element with respect to boron (the B atom bearing a markedly positive charge). The fact that $q$(At) decreases when the SOC is taken into account, supports the lowering of At electronegativity due to the SOC. Otherwise, the SOC effects on both ELF and QTAIM topologies seem rather limited. The extension of the At-bond (about +0.02 Å) due to the SOC is two times less pronounced than for the $AtCH_3$ molecule (+0.04 Å).

Currently, the two most developed approaches for the use of $^{211}$At in targeted alpha therapy are founded on analogies with labeling protocols of iodide disease-targeting carrier biomolecules. They are focused on the formation of either At−C bonds or At−B bonds with bifunctional agents. But unfortunately, most adducts do not provide "adequate" in vivo stability to move into clinical studies,[43,44] too large fractions of $^{211}$At radioisotope being released in the biological medium (this process is referred to as deastatination in the literature). The free At will not reach the targeted cancer cells and may damage healthy tissues. Although the selected model compounds, $AtCH_3$ and $AtBH_2$, represent a substantial simplification of the bifunctional reagents used for $^{211}$At-labeling, some disclosed features may remain and could be helpful for rationalizing some of the experimental results, e.g. the different in vivo stability observed between compounds labeled using either At−C or At−B bond formation.[86,94−97] Indeed, striking differences have been shown regarding the At-bonds in $AtCH_3$ and $AtBH_2$. The At-bond stability depends in one case on CS bonding, i.e. electron pair fluctuations due to the ionic−covalent mixing, while in the other case, the bond stability results from the covalent sharing of the electron pair. Therefore, the two bonds may endure differently the influence of the biological environment. Beyond the different nature of the At−C and At−B bonds, the At atom seems not to behave the same: At is negatively charged in $AtBH_2$ while it is positively charged in $AtCH_3$. Hence, the C−At and B−At bonds are polarized in opposite directions. If this observation remains valid for $^{211}$At-labeled biomolecules, it can definitively imply different behaviors depending on wether the labeling protocol involves an At−C or an At−B bond formation. In the first case, the positive At atom is sensitive to nucleophilic attacks from agents present in the biological environment, while in the second case, the negative At atom is sensitive to electrophilic attacks. Note that numerous experiments have demonstrated different natural degradation pathways between biomolecules labeled using either At−C or At−B bonds formation, on the basis of different biodistributions of the released $^{211}$At radioisotope in selected tissues.[86,94−97]

## 4. CONCLUSION

In this work, we have demonstrated the usefulness of the QTAIM analysis for investigating the electronic structure of heavy-atom systems, where the consideration of SOC is crucial. Indeed, standard QTAIM descriptors such as atomic charges and the Laplacian of the density at the BCP, $\nabla^2\rho_b$, are subject to noticeable modifications that witness the effects of SOC on the molecular bonding. Astatine electronegativity is effectively lowered by SOC and may even lead to an inversion of the dipole moment orientation. The QTAIM classification, limited to shared-shell interactions and closed-shell interactions, fails to characterize the bonding for some At-species. ELF topological analyzes revealed a connection between SOC and the repulsion between the $\sigma$ bonding electrons and the adjacent At lone pair having the same symmetry, known as the lone pair bond-weakening effect (LPBWE). For some At-bonds, SOC leads to an electron population decrease in the bonding region (contributing to the covalent character of the bond), while an increase is observed in the region of At lone pairs mainly perpendicular to the bond, which lowers the LPBWE. Therefore, SOC results in a rise of At propensity to make charge-shift (CS) bonds.

The combination of the QTAIM and ELF topological analyzes was found suitable for characterizing CS bonds involving At atoms, and it was shown in the $AtCH_3$ compound that SOC even changes the nature of the At−C bond from mainly covalent to charge-shift type bonding. This points out that relativistic spin-dependent effects must imperatively be evaluated when interactions between astatine and carbon systems are studied. A different behavior is predicted for the At−B bond in $AtBH_2$. Owning to the key role played by At−C and At−B bonds in the $^{211}$At-labeling protocols currently being developed for nuclear medicine applications, the disparities disclosed between both bond types could explain the greater in vivo stability of the compounds labeled through the formation of an At−B bond. Beyond a practical use for the basic understanding of At chemistry, the introduced topological analysis in the field of quasirelativistic quantum calculations enables an easy investigation of the nature of chemical bonds and interactions in large/complex molecular systems involving (super)heavy atoms. Extending this work to other functions of the electron density (Fukui functions, NCI index), as well as shedding some light on VSEPR distortions in medium-size heavy-atom systems, appears particularly attractive.

## ■ ASSOCIATED CONTENT

### Supporting Information

Two tables reporting additional results from ELF topological analyzes on the $X_2$ and AtX (X = I, Br, Cl, F) species. This material is available free of charge via the Internet at http://pubs.acs.org.

## AUTHOR INFORMATION


### Corresponding Authors

*E-mail: pilme@lct.jussieu.fr (J.P.).
*E-mail: nicolas.galland@univ-nantes.fr (N.G.).


### Notes

The authors declare no competing financial interest.

## ACKNOWLEDGMENTS

This work has been supported by grants funded by the French National Agency for Research (ANR-2010-BLAN-0807-01), with "Investissements d'Avenir" (ANR-11-EQPX-0004, ANR-11-LABX-0018-01), and by the "Région Pays de la Loire" (NUCSAN project). This work has been performed using HPC resources from GENCI-CINES/IDRIS (grant 2013-c2013085117) and CCIPL (Centre de Calcul Intensif des Pays de la Loire).

## REFERENCES


(1) Liu, W. Ideas of relativistic quantum chemistry. *Mol. Phys.* **2010**, *108*, 1679−1706.
(2) Dolg, M.; Cao, X. Relativistic Pseudopotentials: Their Development and Scope of Applications. *Chem. Rev.* **2011**, *112*, 403−480.
(3) Saue, T. Relativistic Hamiltonians for Chemistry: A Primer. *ChemPhysChem* **2011**, *12*, 3077−3094.
(4) Nakajima, T.; Hirao, K. The Douglas−Kroll−Hess Approach. *Chem. Rev.* **2011**, *112*, 385−402.
(5) Fleig, T. Invited review: Relativistic wave-function based electron correlation methods. *Chem. Phys.* **2012**, *395*, 2−15.
(6) Autschbach, J. Perspective: Relativistic effects. *J. Chem. Phys.* **2012**, *136*, 150902.
(7) Liu, W. Advances in relativistic molecular quantum mechanics. *Phys. Rep.* **2014**, *537*, 59−89.
(8) *Relativistic Electronic Structure Theory, Part 2: Applications*; Schwerdtfeger, P., Ed.; Elsevier B. V.: Amsterdam, Netherlands, 2004.
(9) Dyall, K. G.; Faegri, K., Jr. *Introduction to relativistic quantum chemistry*; Oxford University Press, Inc.: New York, USA, 2007; p 453−470.
(10) Visscher, L.; Dyall, K. G. Relativistic and correlation effects on molecular properties. I. The dihalogens F2, Cl2, Br2, I2, and At2. *J. Chem. Phys.* **1996**, *104*, 9040−9046.
(11) Visscher, L.; Styszynski, J.; Nieuwpoort, W. C. Relativistic and correlation effects on molecular properties. II. The hydrogen halides HF, HCl, HBr, HI, and HAt. *J. Chem. Phys.* **1996**, *105*, 1987−1994.
(12) Saue, T.; Faegri, K.; Gropen, O. Relativistic effects on the bonding of heavy and superheavy hydrogen halides. *Chem. Phys. Lett.* **1996**, *263*, 360−366.
(13) van Lenthe, E.; Snijders, J. G.; Baerends, E. J. The zero-order regular approximation for relativistic effects: The effect of spin-orbit coupling in closed shell molecules. *J. Chem. Phys.* **1996**, *105*, 6505−6516.
(14) Nash, C. S.; Bursten, B. E. Spin-Orbit Coupling versus the VSEPR Method: On the Possibility of a Nonplanar Structure for the Super-Heavy Noble Gas Tetrafluoride (118)F4. *Angew. Chem., Int. Ed.* **1999**, *38*, 151−153.
(15) Han, Y.-K.; Lee, Y. S. Structures of RgFn (Rg = Xe, Rn, and Element 118. n = 2, 4.) Calculated by Two-component Spin-Orbit Methods. A Spin-Orbit Induced Isomer of (118)F4. *J. Phys. Chem. A* **1999**, *103*, 1104−1108.
(16) Dyall, K. G. Bond Dissociation Energies of the Tungsten Fluorides and Their Singly Charged Ions: A Density Functional Survey. *J. Phys. Chem. A* **2000**, *104*, 4077−4083.
(17) Faegri, J. K.; Saue, T. Diatomic molecules between very heavy elements of group 13 and group 17: A study of relativistic effects on bonding. *J. Chem. Phys.* **2001**, *115*, 2456−2464.
(18) Dubillard, S.; Rota, J. B.; Saue, T.; Faegri, K. Bonding analysis using localized relativistic orbitals: Water, the ultrarelativistic case and the heavy homologues H2X (X = Te, Po, eka-Po). *J. Chem. Phys.* **2006**, *124*, 154307.
(19) Rusakov, A. A.; Rykova, E.; Scuseria, G. E.; Zaitsevskii, A. Importance of spin-orbit effects on the isomerism profile of Au3: An ab initio study. *J. Chem. Phys.* **2007**, *127*, 164322.
(20) Kim, H.; Choi, Y. J.; Lee, Y. S. Spin-Orbit and Electron Correlation Effects on the Structure of EF3 (E = I, At, and Element 117). *J. Phys. Chem. B* **2008**, *112*, 16021−16029.
(21) Alvarez-Thon, L.; David, J.; Arratia-Pérez, R.; Seppelt, K. Ground state of octahedral platinum hexafluoride. *Phys. Rev. A* **2008**, *77*, 034502.
(22) Opalka, D.; Segado, M.; Poluyanov, L. V.; Domcke, W. Relativistic Jahn-Teller effect in tetrahedral systems. *Phys. Rev. A* **2010**, *81*, 042501.
(23) Wedig, U.; Saltykov, V.; Nuss, J.; Jansen, M. Homoatomic Stella Quadrangula [Tl8]6− in Cs18Tl8O6, Interplay of Spin−Orbit Coupling, and Jahn−Teller Distortion. *J. Am. Chem. Soc.* **2010**, *132*, 12458−12463.
(24) Baldes, A.; Gulde, R.; Weigend, F. Jahn−Teller Distortion Versus Spin−Orbit Splitting: Symmetry of Small Heavy-Metal Atom Clusters. *J. Clust Sci.* **2011**, *22*, 355−363.
(25) Yang, D.-D.; Wang, F. Structures and stabilities of group 17 fluorides EF3 (E = I, At, and element 117) with spin-orbit coupling. *Phys. Chem. Chem. Phys.* **2012**, *14*, 15816−15825.
(26) Gagliardi, L.; Roos, B. O. Quantum chemical calculations show that the uranium molecule U2 has a quintuple bond. *Nature* **2005**, *433*, 848−851.
(27) Aquino, F.; Govind, N.; Autschbach, J. Electric Field Gradients Calculated from Two-Component Hybrid Density Functional Theory Including Spin−Orbit Coupling. *J. Chem. Theory Comput.* **2010**, *6*, 2669−2686.
(28) Vallet, V.; Wahlgren, U.; Grenthe, I. Probing the Nature of Chemical Bonding in Uranyl(VI) Complexes with Quantum Chemical Methods. *J. Phys. Chem. A* **2012**, *116*, 12373−12380.
(29) Sattelberger, A. P.; Johnson, M. J. A. Uncovering the Uranium-Nitrogen Triple Bond. *Science* **2012**, *337*, 652−653.
(30) Christiansen, P. A.; Pitzer, K. S. Electronic structure and dissociation curves for the ground states of Tl2 and Tl2[+] from relativistic effective potential calculations. *J. Chem. Phys.* **1981**, *74*, 1162−1165.
(31) Dyall, K. G. All-electron molecular Dirac–Hartree–Fock calculations: Properties of the group IV monoxides GeO, SnO, and PbO. *J. Chem. Phys.* **1993**, *98*, 2191−2197.
(32) *TURBOMOLE*, v6.3.1; a development of University of Karlsruhe and Forschungszentrum Karlsruhe GmbH, TURBOMOLE GmbH: Karlsruhe, Germany, 2011.
(33) Zeng, T.; Fedorov, D. G.; Schmidt, M. W.; Klobukowski, M. Effects of Spin−Orbit Coupling on Covalent Bonding and the Jahn−Teller Effect Are Revealed with the Natural Language of Spinors. *J. Chem. Theory Comput.* **2011**, *7*, 2864−2875.
(34) Becke, A. D.; Edgecombe, K. E. A simple measure of electron localization in atomic and molecular systems. *J. Chem. Phys.* **1990**, *92*, 5397−5403.
(35) Silvi, B.; Savin, A. Classification of chemical bonds based on topological analysis of electron localization functions. *Nature* **1994**, *371*, 683−686.
(36) Piquemal, J. P.; Pilmé, J.; Parisel, O.; Gérard, H.; Fourré, I.; Bergès, J.; Gourlaouen, C.; De La Lande, A.; Van Severen, M. C.; Silvi, B. What can be learnt on biologically relevant systems from the topological analysis of the electron localization function? *Int. J. Quantum Chem.* **2008**, *108*, 1951−1969.
(37) de Courcy, B.; Pedersen, L. G.; Parisel, O.; Gresh, N.; Silvi, B.; Pilmé, J.; Piquemal, J. P. Understanding Selectivity of Hard and Soft Metal Cations within Biological Systems Using the Subvalence Concept. 1. Application to Blood Coagulation: Direct Cation−Protein Electronic Effects versus Indirect Interactions through Water Networks. *J. Chem. Theory Comput.* **2010**, *6*, 1048−1063.
(38) Pilmé, J.; Renault, E.; Ayed, T.; Montavon, G.; Galland, N. Introducing the ELF Topological Analysis in the Field of

Quasirelativistic Quantum Calculations. *J. Chem. Theory Comput.* **2012**, *8*, 2985−2990.
(39) Bader, R. F. W.; Beddall, P. M. Virial partitioning of charge distributions and properties of diatomic hydrides. *J. Am. Chem. Soc.* **1973**, *95*, 305−315.
(40) Bader, R. F. W. *Atoms in Molecules: A Quantum Theory*; Oxford University Press: New York, USA, 1994.
(41) Eickerling, G.; Mastalerz, R.; Herz, V.; Scherer, W.; Himmel, H.-J.; Reiher, M. Relativistic Effects on the Topology of the Electron Density. *J. Chem. Theory Comput.* **2007**, *3*, 2182−2197.
(42) Matito, E.; Salvador, P.; Styszynski, J. Benchmark calculations of metal carbonyl cations: relativistic vs. electron correlation effects. *Phys. Chem. Chem. Phys.* **2013**, *15*, 20080−20090.
(43) Wilbur, D. S. [211At]astatine-labeled compound stability: issues with released [211At]astatide and development of labeling reagents to increase stability. *Curr. Radiopharm.* **2008**, *1*, 144−176.
(44) Vaidyanathan, G.; Zalutsky, M. R. Astatine radiopharmaceuticals: prospects and problems. *Curr. Radiopharm.* **2008**, *1*, 177−196.
(45) Wilbur, D. S. Enigmatic astatine. *Nat. Chem.* **2013**, *5*, 246−246.
(46) Champion, J.; Seydou, M.; Sabatie-Gogova, A.; Renault, E.; Montavon, G.; Galland, N. Assessment of an effective quasirelativistic methodology designed to study astatine chemistry in aqueous solution. *Phys. Chem. Chem. Phys.* **2011**, *13*, 14984−14992.
(47) Fleig, T.; Sadlej, A. J. Electric dipole polarizabilities of the halogen atoms in 2P1/2 and 2P3/2 states: Scalar relativistic and two-component configuration-interaction calculations. *Phys. Rev. A* **2002**, *65*, 032506.
(48) Ayed, T.; Seydou, M.; Réal, F.; Montavon, G.; Galland, N. How Does the Solvation Unveil AtO+ Reactivity? *J. Phys. Chem. B* **2013**, *117*, 5206−5211.
(49) Hermann, A.; Hoffmann, R.; Ashcroft, N. W. Condensed Astatine: Monatomic and Metallic. *Phys. Rev. Lett.* **2013**, *111*, 116404.
(50) Gomes, A. S. P.; Real, F.; Galland, N.; Angeli, C.; Cimiraglia, R.; Vallet, V. Electronic structure investigation of the evanescent AtO+ ion. *Phys. Chem. Chem. Phys.* **2014**, *16*, 9238−9248.
(51) Han, Y.-K.; Bae, C.; Son, S.-K.; Lee, Y. S. Spin-orbit effects on the transactinide p-block element monohydrides MH (M=element 113−118). *J. Chem. Phys.* **2000**, *112*, 2684−2691.
(52) Straatsma, T. P.; Aprà, E.; Windus, T. L.; Bylaska, E. J.; de Jong, W.; Hirata, S.; Valiev, M.; Hackler, M.; Pollack, L.; Harrison, R. et al. *NWChem, A Computational Chemistry Package for Parallel Computers*, version 5.1.1; Pacific Northwest National Laboratory: Richland, WA, 2008.
(53) Bader, R. F. W.; Beddall, P. M.; Cade, P. E. Partitioning and characterization of molecular charge distributions. *J. Am. Chem. Soc.* **1971**, *93*, 3095−3107.
(54) Pilmé, J.; Piquemal, J.-P. Advancing beyond charge analysis using the electronic localization function: Chemically intuitive distribution of electrostatic moments. *J. Comput. Chem.* **2008**, *29*, 1440−1449.
(55) Ponec, R.; Uhlik, F. Electron pairing and chemical bonds. On the accuracy of the electron pair model of chemical bond. *J. Mol. Struct.* **1997**, *391*, 159−168.
(56) Matta, C. F.; Boyd, R. J. In *The Quantum Theory of Atoms in Molecules*; Matta, C. F., Boyd, R. J., Eds.; Wiley-VCH Verlag GmbH & Co. KGaA: Weinheim, Germany, 2007; p 1−34.
(57) Bader, R. F. W.; Essén, H. The characterization of atomic interactions. *J. Chem. Phys.* **1984**, *80*, 1943−1960.
(58) Cremer, D.; Kraka, E. Chemical Bonds without Bonding Electron Density — Does the Difference Electron-Density Analysis Suffice for a Description of the Chemical Bond? *Angew. Chem., Int. Ed.* **1984**, *23*, 627−628.
(59) Nakanishi, W.; Hayashi, S. Role of dG/dw and dV/dw in AIM Analysis: An Approach to the Nature of Weak to Strong Interactions. *J. Phys. Chem. A* **2013**, *117*, 1795−1803.
(60) Llusar, R.; Beltrán, A.; Andrés, J.; Noury, S.; Silvi, B. Topological analysis of electron density in depleted homopolar chemical bonds. *J. Comput. Chem.* **1999**, *20*, 1517−1526.
(61) Pilme, J.; Silvi, B.; Alikhani, M. E. Comparative Study of the Bonding in the First Series of Transition Metal 1:1 Complexes M−L (M = Sc, ..., Cu; L = CO, N2, C2H2, CN-, NH3, H2O, and F-). *J. Phys. Chem. A* **2005**, *109*, 10028−10037.
(62) Shaik, S.; Danovich, D.; Silvi, B.; Lauvergnat, D. L.; Hiberty, P. C. Charge-Shift Bonding-A Class of Electron-Pair Bonds That Emerges from Valence Bond Theory and Is Supported by the Electron Localization Function Approach. *Chem.—Eur. J.* **2005**, *11*, 6358−6371.
(63) Choi, Y. J.; Lee, Y. S. Spin-orbit density functional theory calculations for heavy metal monohydrides. *J. Chem. Phys.* **2003**, *119*, 2014−2019.
(64) Champion, J.; Alliot, C.; Renault, E.; Mokili, B. M.; Cherel, M.; Galland, N.; Montavon, G. Astatine Standard Redox Potentials and Speciation in Acidic Medium. *J. Phys. Chem. A* **2010**, *114*, 576−582.
(65) Champion, J.; Sabatié-Gogova, A.; Bassal, F.; Ayed, T.; Alliot, C.; Galland, N.; Montavon, G. Investigation of Astatine (III) Hydrolyzed Species: Experiments and Relativistic Calculations. *J. Phys. Chem. A* **2013**, *117*, 1983−1990.
(66) Peterson, K. A.; Figgen, D.; Goll, E.; Stoll, H.; Dolg, M. Systematically convergent basis sets with relativistic pseudopotentials. II. Small-core pseudopotentials and correlation consistent basis sets for the post-d group 16−18 elements. *J. Chem. Phys.* **2003**, *119*, 11113−11123.
(67) Peterson, K. A.; Shepler, B. C.; Figgen, D.; Stoll, H. On the Spectroscopic and Thermochemical Properties of ClO, BrO, IO, and Their Anions. *J. Phys. Chem. A* **2006**, *110*, 13877−13883.
(68) Bischoff, F. A.; Klopper, W. Second-order electron-correlation and self-consistent spin-orbit treatment of heavy molecules at the basis-set limit. *J. Chem. Phys.* **2010**, *132*, 094108.
(69) Armbruster, M. K.; Klopper, W.; Weigend, F. Basis-set extensions for two-component spin-orbit treatments of heavy elements. *Phys. Chem. Chem. Phys.* **2006**, *8*, 4862−4865.
(70) Dunning, T. H., Jr. Gaussian basis sets for use in correlated molecular calculations. I. The atoms boron through neon and hydrogen. *J. Chem. Phys.* **1989**, *90*, 1007−1023.
(71) Kendall, R. A.; Dunning, T. H., Jr.; Harrison, R. J. Electron affinities of the first-row atoms revisited. Systematic basis sets and wave functions. *J. Chem. Phys.* **1992**, *96*, 6796−6806.
(72) Woon, D. E.; Dunning, T. H., Jr. Gaussian basis sets for use in correlated molecular calculations. III. The atoms aluminum through argon. *J. Chem. Phys.* **1993**, *98*, 1358−1371.
(73) Stephens, P. J.; Devlin, F. J.; Chabalowski, C. F.; Frisch, M. J. Ab Initio Calculation of Vibrational Absorption and Circular Dichroism Spectra Using Density Functional Force Fields. *J. Phys. Chem.* **1994**, *98*, 11623−11627.
(74) Nakajima, T.; Hirao, K. Extended Douglas-Kroll transformations applied to the relativistic many-electron Hamiltonian. *J. Chem. Phys.* **2003**, *119*, 4105−4111.
(75) Mitin, A. V.; van Wullen, C. Two-component relativistic density-functional calculations of the dimers of the halogens from bromine through element 117 using effective core potential and all-electron methods. *J. Chem. Phys.* **2006**, *124*, 64305.
(76) Noury, S.; Krokidis, X.; Fuster, F.; Silvi, B. Computational tools for the electron localization function topological analysis. *Comput. Chem.* **1999**, *23*, 597−604.
(77) Flukiger, P.; Luthi, H. P.; Portmann, S.; Weber, J. *Molekel*, version 4.3; Swiss Center for Scientific Computing: Manno, Switzerland, 2002.
(78) Dennington, R.; Keith, T.; Millam, J. *GaussView*, version 5.0.9; Semichem Inc.: Shawnee Mission KS, USA, 2009.
(79) Peng, D.; Liu, W.; Xiao, Y.; Cheng, L. Making four- and two-component relativistic density functional methods fully equivalent based on the idea of "from atoms to molecule". *J. Chem. Phys.* **2007**, *127*, 104106.
(80) Pauling, L. *The Nature of the Chemical Bond*; Cornell University Press: Ithaca, NY, 1939.

(81) Shaik, S.; Danovich, D.; Wu, W.; Hiberty, P. C. Charge-shift bonding and its manifestations in chemistry. *Nat. Chem.* **2009**, *1*, 443−449.
(82) Zhang, L.; Ying, F.; Wu, W.; Hiberty, P. C.; Shaik, S. Topology of Electron Charge Density for Chemical Bonds from Valence Bond Theory: A Probe of Bonding Types. *Chem.—Eur. J.* **2009**, *15*, 2979−2989.
(83) Appelman, E. H. Solvent-extraction studies of interhalogen compounds of astatine. *J. Phys. Chem.* **1961**, *65*, 325−331.
(84) Appelman, E. H.; Sloth, E. N.; Studier, M. H. Observation of astatine compounds by time-of-flight mass spectrometry. *Inorg. Chem.* **1966**, *5*, 766−769.
(85) Hill, J. G.; Hu, X. Theoretical Insights into the Nature of Halogen Bonding in Prereactive Complexes. *Chem.—Eur. J.* **2013**, *19*, 3620−3628.
(86) Steffen; Almqvist; Chyan; Lundqvist; Tolmachev; Wilbur; Carlsson. Biodistribution of 211At labeled HER-2 binding affibody molecules in mice. *Oncol. Rep.* **2007**, *17*, 1141−1147.
(87) Sanderson, R. T. *Polar covalence*; Academic Press: New York, USA, 1983.
(88) Gomes, A. S. P.; Visscher, L. The influence of core correlation on the spectroscopic constants of HAt. *Chem. Phys. Lett.* **2004**, *399*, 1−6.
(89) Norman, P.; Schimmelpfennig, B.; Ruud, K.; Jensen, H. J. A.; Agren, H. Relativistic effects on linear and nonlinear polarizabilities studied by effective-core potential, Douglas-Kroll, and Dirac-Hartree-Fock response theory. *J. Chem. Phys.* **2002**, *116*, 6914−6923.
(90) Dolg, M. Accuracy of energy-adjusted quasi-relativistic pseudopotentials: a calibration study of XH and X2 (X = F, Cl, Br, I, At). *Mol. Phys.* **1996**, *88*, 1645−1655.
(91) Corson, D. R.; MacKenzie, K. R.; Segrè, E. Possible Production of Radioactive Isotopes of Element 85. *Phys. Rev.* **1940**, *57*, 459−459.
(92) Hamilton, J. G.; Soley, M. H. A Comparison of the Metabolism of Iodine and of Element 85 (Eka-Iodine). *Proc. Natl. Acad. Sci. U. S. A.* **1940**, *26*, 483−489.
(93) Alkorta, I.; Blanco, F.; Solimannejad, M.; Elguero, J. Competition of Hydrogen Bonds and Halogen Bonds in Complexes of Hypohalous Acids with Nitrogenated Bases. *J. Phys. Chem. A* **2008**, *112*, 10856−10863.
(94) Wilbur, D. S.; Chyan, M.-K.; Hamlin, D. K.; Kegley, B. B.; Risler, R.; Pathare, P. M.; Quinn, J.; Vessella, R. L.; Foulon, C.; Zalutsky, M.; et al. Reagents for Astatination of Biomolecules: Comparison of the in Vivo Distribution and Stability of Some Radioiodinated/Astatinated Benzamidyl and nido-Carboranyl Compounds. *Bioconjugate Chem.* **2004**, *15*, 203−223.
(95) Wilbur, D. S.; Hamlin, D. K.; Chyan, M.-K.; Kegley, B. B.; Quinn, J.; Vessella, R. L. Biotin Reagents in Antibody Pretargeting. 6. Synthesis and in Vivo Evaluation of Astatinated and Radioiodinated Aryl- and nido-Carboranyl-biotin Derivatives. *Bioconjugate Chem.* **2004**, *15*, 601−616.
(96) Wilbur, D. S.; Chyan, M.-K.; Hamlin, D. K.; Vessella, R. L.; Wedge, T. J.; Hawthorne, M. F. Reagents for Astatination of Biomolecules. 2. Conjugation of Anionic Boron Cage Pendant Groups to a Protein Provides a Method for Direct Labeling that is Stable to in Vivo Deastatination. *Bioconjugate Chem.* **2007**, *18*, 1226−1240.
(97) Yang, Y.; Lin, R.; Liu, N.; Liao, J.; Wei, M.; Jin, J. Astatine-211 labeling of protein using TCP as a bi-functional linker: synthesis and preliminary evaluation in vivo and in vitro. *J. Radioanal. Nucl. Chem.* **2011**, *288*, 71−77.